11th World Congress on Computational Mechanics (WCCM XI)
5th European Conference on Computational Mechanics (ECCM V)
6th European Conference on Computational Fluid Dynamics (ECFD VI)
E. Oñate, J. Oliver and A. Huerta (Eds)

# LES OF WIND AND WAVE FORCED OCEANIC TURBULENT BOUNDARY LAYERS USING THE RESIDUAL-BASED VARIATIONAL MULTISCALE METHOD AND NEAR-WALL MODELING

**ANDRES E. TEJADA-MARTINEZ*, ROOZBEH GOLSHAN*, IDO AKKERMAN† and YURI BAZILEVS††**

*Department of Civil and Environmental Engineering
University of South Florida
4202 East Fowler Avenue ENB 118
Tampa, FL 33620, USA
e-mail: aetejada@usf.edu, rgolshan@mail.usf.edu

†School of Engineering and Computing Sciences
Durham University
South Road, DH1 3LE
Durham, UK
e-mail: ido.akkerman@durham.ac.uk

††Department of Structural Engineering
University of California, San Diego
9500 Gilman Drive MC0085
La Jolla, CA 92093, USA
e-mail: yuri@ucsd.edu

**Key words:** Langmuir Turbulence, Langmuir Circulation, Wall Modeling, Residual-based Variational Multiscale Method

**Abstract.** Large-eddy simulation (LES) of wind and wave forced oceanic turbulent boundary layers is performed using the residual-based variational multiscale method (RBVMS) [1, 10] and near-wall modeling [2, 9]. Wind and surface gravity wave forcing generates Langmuir turbulence characterized by Langmuir circulation (LC) with largest scales consisting of streamwise vortices aligned in the direction of the wind, acting as a secondary flow structure to the primary wind-driven component of the flow. Our LES is representative of a shallow water continental shelf flow (10 to 30 meters in depth) far from lateral boundaries in which LC engulfs the full depth of the water column and disrupts the bottom log layer. Field measurements indicate that occurrence of full-depth LC is typical during the passage of storms. The RBVMS method with quadratic NURBS (Non-Uniform Rational B-splines) with near-wall resolution has been shown to possess good convergence characteristics for this flow [10]. The use of near-wall modeling facilitates

simulations with expanded domains over horizontal directions. Thus, these simulations are able to resolve multiple Langmuir cells permitting analysis of the interaction between the cells. Results in terms of velocity statistics are presented from simulations performed with various domain sizes and distinct near-wall treatments: (1) the classical treatment reviewed in [9] based on prescription of the wall shear stress and (2) a recent treatment presented in [2] based on weak imposition of the no-slip bottom boundary condition.

## 1 INTRODUCTION

Wind speeds greater than 3 m $s^{-1}$ can lead to the generation of Langmuir turbulence in the upper ocean [11]. Interaction between surface gravity waves and the wind-driven shear current in the upper ocean is well-known to produce Langmuir turbulence characterized by Langmuir circulation or cells consisting of parallel counter-rotating vortices roughly aligned in the direction of the wind. The longest Langmuir cells extend in the downwind direction for tens of meters to kilometers. In the upper ocean mixed layer, the cells can extend to the base of the mixed layer which is tens of meters deep, depending on various factors such as winds, surface waves and surface buoyancy conditions. In shallow coastal shelf regions, the passage of storms leads to intense vertical mixing and an unstratified water column. In these cases, Langmuir cells have been observed occupying the full-depth of the water column while serving as an important mechanism for sediment re-suspension [5, 6]. Full-depth Langmuir cells have been observed in water columns ranging from 10 to 30 meters deep.

Over the past two decades LES has yielded fundamental knowledge on the structure of Langmuir turbulence. These simulations have been based on the phase-averaged Navier-Stokes equations or Craik-Leibovich equations [7] in which the averaging filters out surface gravity waves giving rise to the well-known Craik-Leibovich (C-L) vortex force [4]. The C-L vortex force consists of the cross-product between the Stokes drift velocity induced by surface gravity waves and the flow vorticity. The presence of this force in the momentum equations accounts for the generating mechanism of Langmuir turbulence without the need to resolve surface gravity waves. Hence, simulations may be conducted with a flat surface.

In [10] we have shown that the C-L vortex force in the Craik-Leibovich equations possesses an advective structure given in terms of an advective matrix of velocities. Such advective structure led to the consistent definition of the intrinsic timescale parameter $\tau_M$ for the momentum equation in the RBVMS formulation of the C-L equations. Furthermore, in [10] we performed LES with near-wall resolution (LES-NWR) of Langmuir turbulence in shallow water characterized by full-depth Langmuir cells. Results from the simulations compared favorably with the field measurements of [5, 6] in terms of the turbulence structure resolved.

The LES of [10] was performed with relatively small domain dimensions in the stream-

wise (downwind) and spanwise (crosswind) directions and thus limited to resolution of one full-depth Langmuir cell. In this paper, we make use of the formulation in [10] together with near-wall modeling in order to perform simulations on bigger domains over downwind and crosswind directions and thus investigate the impact of the domain size on the resolved Langmuir turbulence structure and statistics. Such simulation approach is often referred to as LES with near-wall modeling or LES-NWM and permits simulations without having to resolve the computationally expensive near-wall region.

## 2 COMPUTATIONAL SETUP

The computational domain is similar to that depicted in [10] and consists of a rectangular box with dimensions $L_1$ in the streamwise or downwind ($x_1$) direction, $L_2$ in the spanwise or crosswind ($x_2$) direction and $L_3$ in the vertical or wall-normal ($x_3$) direction.

The half-depth of the domain (in the $x_3$-direction) is $\delta$ and the domain extends from 0 to $2\delta$ over $x_3$. Various domain lengths over $x_1$ and $x_2$ directions were utilized in order to investigate their influence on turbulence structure and statistics. Domain sizes are listed in Table 1. This table also shows mesh resolutions in terms of the numbers of quadratic NURBS basis functions ($N_1$, $N_2$ and $N_3$) used in each tensor product direction. Mesh resolution is uniform in all three directions. The coarse mesh resolution in the wall-normal (vertical) is such that viscous wall and buffer sublayers are not well-resolved, thereby requiring near-wall modeling.

| $L_1$ | $L_2$ | $L_3$ | $N_1$ | $N_2$ | $N_3$ |
|---|---|---|---|---|---|
| $4\pi\delta$ | $\frac{8}{3}\pi\delta$ | $2\delta$ | 32 | 64 | 34 |
| $28\pi\delta$ | $\frac{16}{3}\pi\delta$ | $2\delta$ | 256 | 128 | 34 |
| $40\pi\delta$ | $\frac{16}{3}\pi\delta$ | $2\delta$ | 320 | 128 | 34 |

**Table 1**: Summary of domain sizes and mesh resolutions used in LES-NWM.

The flow is driven by a constant wind stress $\tau_w = \rho u_\tau^2$, where $\rho$ is density and $u_\tau$ is wind stress friction velocity. This wind stress is applied in the $x_1$ direction at the top surface ($x_3 = 2\delta$) of the rectangular box domain, where no-penetration boundary condition is also assumed to hold. A no-slip condition (enforced weakly) or a shear stress (a Neumman boundary condition) is applied at the bottom wall boundary ($x_3 = 0$). In the streamwise and spanwise directions, periodic boundary conditions are employed in order to represent an unbounded domain in these directions, approximating a continental shelf wind and wave-driven flow far from (unaffected by) coastal boundaries.

Characteristic flow velocity, Stokes drift velocity and length are taken as wind stress friction velocity $u_\tau$, Stokes drift at the surface $u_s$, and half-depth $\delta$, respectively. Characteristic time scale is taken as $\delta/u_\tau$. Using these scales to non-dimensionalize the Craik-Leibovich equations gives rise to the Reynolds number defined as $Re = u_\tau\delta/\nu$ (where $\nu$ is kinematic viscosity) and the turbulent Langmuir number defined as $La_t = \sqrt{u_\tau/u_s}$,

the latter representative of wind forcing relative to wave forcing. Note that the C-L vortex force in the momentum (Craik-Leibovich) equations requires input of the Stokes drift velocity which is a depth-dependent ($x_3$) function decaying with distance to the top surface of the domain. The decay rate is inversely proportional to $\lambda$, the wavelength of the dominant surface gravity waves generating the Langmuir turbulence (thus the Stokes drift velocity decays with depth more rapidly for shorter waves). The interested reader is directed to [10] for the full Craik-Leibovich equations and corresponding RBVMS formulation. Results presented in upcoming sections were obtained from simulations performed with $Re = 395$, $La_t = 0.7$ and $\lambda = 12\delta$, the latter two parameters representative of the wave and wind forcing conditions during field measurements of full-depth Langmuir cells in [5, 6]. In [12, 10], velocity fluctuations in the core region of the flow obtained from LES-NWR at the laboratory-scale $Re = 395$ have been shown to scale-up favorably to field-scale $Re$ via comparisons with the field measurements in [5, 6]. However, future simulations should be conducted at higher Reynolds numbers to further verify this.

## 3 WALL MODELING

### 3.1 Classical wall model

LES-NWM is performed with two distinct wall modeling approaches. The first is the classical approach in which a Neumann or natural boundary condition is imposed at the bottom wall (at $x_3 = 0$) in the form of the wall shear stress. For example, in this case the dimensional wall shear stress in the $x_1$-momentum equation is prescribed as

$$\tau_{wall} = \rho\, u_*^2\, \frac{u_1(x_1, x_2, x_3^{\mathrm{ol}}, t)}{U^{\mathrm{ol}}} \tag{1}$$

In the previous expression $u_*$ is the wall friction velocity, and $x_3^{\mathrm{ol}}$ denotes the distance from the wall to the first grid point in the outer layer (ol) satisfying the classical logarithmic profile

$$U^{\mathrm{ol}+} = \frac{U^{\mathrm{ol}}}{u_*} = \frac{1}{\kappa}\log\frac{x_3^{\mathrm{ol}} u_*}{\nu} + B \tag{2}$$

Here $\nu$ is kinematic viscosity, $\kappa = 0.41$ is the von Karman constant and $B$ ranges between 5 and 8 for flows with full-depth Langmuir circulation depending on wind and wave forcing conditions (i.e. values of $La_t$ and $\lambda$). The latter variation in $B$ can be observed in the LES-NWR in [13] conducted using a high order hybrid finite difference/spectral numerical method. The wall friction velocity $u_*$ in (1) is solved iteratively from the log law in (2) with $U^{\mathrm{ol}}$ obtained from the LES-computed velocity at $x_3 = x_3^{\mathrm{ol}}$. Note that for the current flow configuration, in the mean, wall friction velocity $u_*$ is equal to wind stress friction velocity $u_\tau$.

### 3.2 Weak imposition of the bottom no-slip condition

An alternate approach to wall modeling has been investigated consisting of weak imposition of the bottom no-slip (Dirichlet) boundary condition. Here the weak Dirichlet boundary terms of the RBVMS formulation are taken as

$$\begin{aligned} B_{wbc}(\{\mathbf{w}\},\{\mathbf{u}\}) = (\mathbf{w}, -2Re^{-1}\nabla^s\mathbf{u}\cdot\mathbf{n})_{\Gamma_g} \\ +(-2Re^{-1}\nabla^s\mathbf{w}\cdot\mathbf{n}, (\mathbf{u}-\mathbf{g}))_{\Gamma_g} \\ +(\mathbf{w}, \tau_B(\mathbf{u}-\mathbf{g}))_{\Gamma_g}, \end{aligned} \tag{3}$$

weakly imposing the Dirichlet boundary condition $\mathbf{u} = \mathbf{g}$, with $\mathbf{u} = (u_1, u_2, u_3)$ being the flow velocity, $\mathbf{w}$ the corresponding weighting function, and $\mathbf{g} = \mathbf{0}$ the no-slip condition at the bottom wall. In equation (3), $\Gamma_g$ is the Dirichlet part of the problem domain boundary (i.e. the bottom wall) and $\mathbf{n}$ is the unit outward normal vector to this boundary (i.e. $(0, 0, -1)$). In the formulation we assume that the normal component of the flow velocity vector (i.e. the wall-normal velocity) is imposed strongly at the boundary (i.e. $u_3 = 0$ strongly at the bottom wall). To ensure numerical stability and optimal convergence, the penalty parameter $\tau_B$ in equation (3) is chosen as

$$\tau_B = C_b Re^{-1}\sqrt{n_i G_{ij} n_j}, \tag{4}$$

where $n_i$'s are the Cartesian component of the unit outward normal vector to $\Gamma_g$ and $C_b$ is an element-wise constant emanating from a boundary inverse estimate [3]. Further discussion and computational results employing weakly-enforced Dirichlet conditions may be found in [2].

## 4 RESULTS

Figure (1) shows velocity fluctuations averaged over the streamwise ($x_1$) direction and over time on the streamwise-wall-normal plane. These averaged fluctuations reveal the cellular structure captured by the LES. In this case, one Langmuir cell was resolved with spanwise length of the domain $L_2 = 8\pi\delta/3$. This spanwise length of the cell is consistent with the field measurements in [5, 6]. In the upper panel of Figure (1), the bottom convergence of the resolved Langmuir cell is seen in terms of converging averaged spanwise velocity fluctuations near $x_2/\delta = 4.2$ in the lower half of the domain. This cell bottom convergence generates the full-depth upwelling limb of the cell, seen in the middle panel of Figure (1) in terms of positive averaged wall-normal velocity fluctuation. Finally, the upwelling limb of the cell generally coincides with a full-depth region of negative averaged streamwise velocity fluctuation (lower panel) which is intensified in the lower half of the domain and in the near-surface region. The previous characteristics are typical of full-depth Langmuir cells as observed in the field measurements in [5, 6].

In Figure (2), the structure of the Langmuir cells is seen in the horizontal (streamwise-spanwise) ($x_1-x_2$) plane at mid-depth ($x_3 = \delta$) of the domain. Here instantaneous streamwise and wall-normal velocity fluctuations are characterized by downwind-elongated streaks

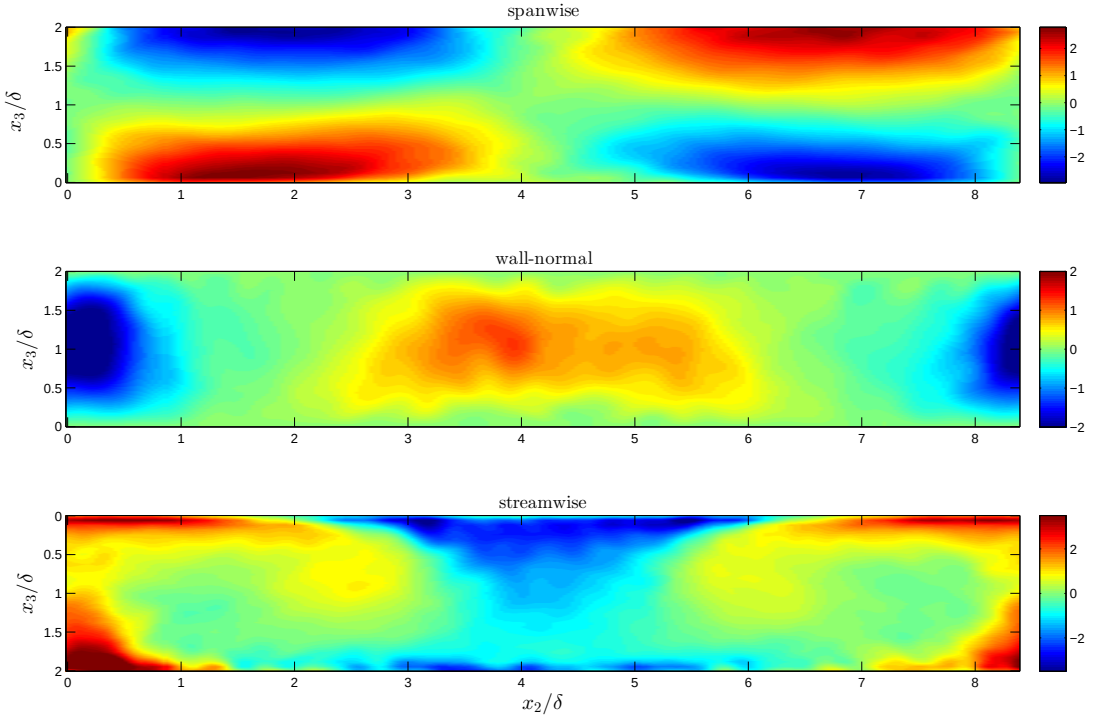


**Figure 1**: Streamwise-wall-normal plane of streamwise- and time-averaged spanwise (top), wall-normal (middle) and streamwise (bottom) velocity fluctuations scaled by $u_\tau$ from LES-NWM in the domain $L_1/\delta \times L_2/\delta \times L_3/\delta = 4\pi \times \frac{8}{3}\pi \times 2$. Results were obtained with classical wall model in sub-section 3.1 with $B = 6.5$ in (2). Streamwise direction ($x_1$) is out of page.

alternating in sign in the spanwise direction. Note that the negative streamwise velocity fluctuation streak (upper panel) corresponds to the upwelling limb of the cell observed earlier in Figure (1). Furthermore in Figure (2), the positive wall-normal velocity fluctuation streak (lower panel) generally coincides with the negative downwind velocity fluctuation streak (upper panel), also consistent with Figure (1).

Figure (3) shows instantaneous streamwise and wall-normal velocity fluctuation streaks at mid-depth in LES-NWM with the domain expanded to $L_1 = 40\pi\delta$ and $L_2 = 16\pi\delta/3$ compared to $L_1 = 4\pi\delta$ and $L_2 = 8\pi\delta/3$ in Figure (2). The expanded domain is able to resolve three Langmuir cells, as can be seen by the three pairs of positive and negative downwind-elongated streaks characterizing the instantaneous streamwise and wall-normal velocity fluctuations. Furthermore, the expanded streamwise length of the domain allows for the cells to interact with each other. Such interaction gives rise to cell meanderings and mergings as is seen in Figure (3). The merging of cells is often observed during field occurrences of Langmuir cells and is typically referred to as a "y-junction" [11].

Figure (4) shows mean velocity in LES-NWM with the classical wall model of subsection 3.1 on the different domains listed earlier in Table 1. The mean velocity in plus

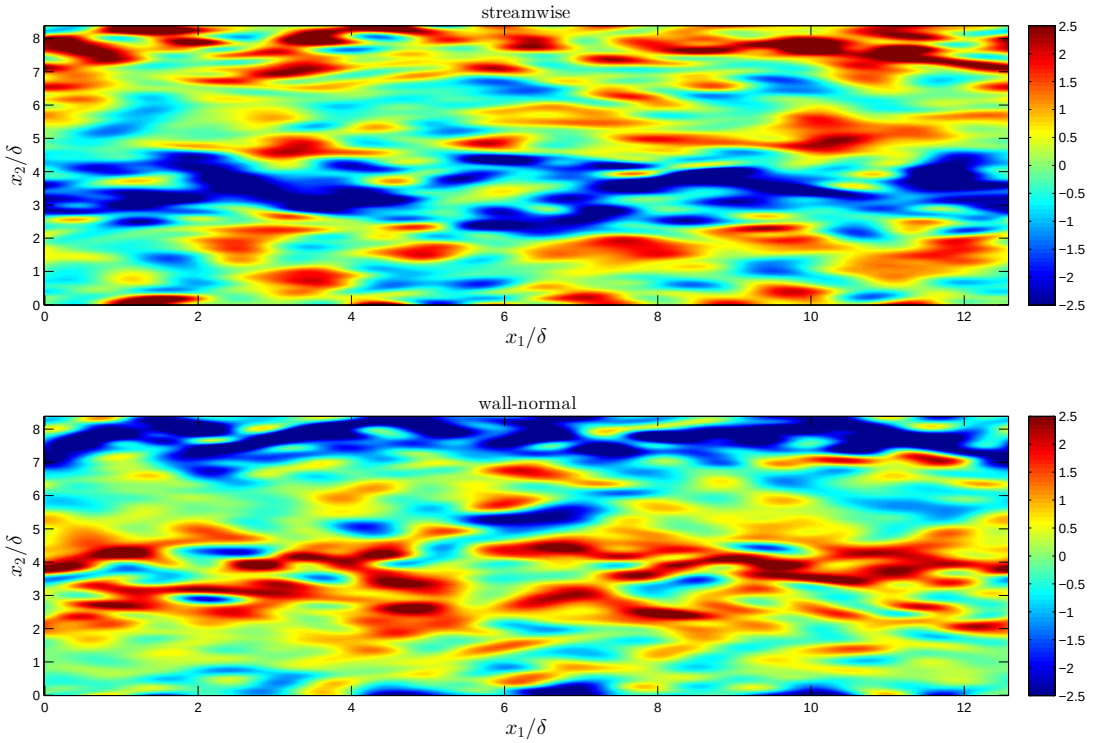


**Figure 2**: Mid-depth ($x_3 = \delta$) streamwise-spanwise plane of instantaneous streamwise (top) and wall-normal (bottom) velocity fluctuations scaled by $u_\tau$ from LES-NWM in the domain $L_1/\delta \times L_2/\delta \times L_3/\delta = 4\pi \times \frac{8}{3}\pi \times 2$. Results were obtained with classical wall model in sub-section 3.1 with $B = 6.5$ in (2).

units is characterized by a deviation from the log-law. This deviation has been attributed to the high speed fluid brought down to the near-wall region by the downwelling limbs of the Langmuir cells [13]. Thus, the log-law deviation depends on the strength of these limbs, which can be measured, for example, in terms of root mean square of wall-normal velocity [8]. As can be seen in Figure (4), the deviation from the log law is robust across LES-NWM with different horizontal domain lengths. Furthermore, all LES-NWM cases predict a mean velocity in good agreement with the velocity calculated via LES-NWR (in [10]) on the smallest domain in Table 1. In [10] LES-NWR (i.e. LES with near-wall resolution) was performed with quadratic NURBS with $N_1 = N_2 = 64$ and $N_3 = 66$. The LES-NWR mesh was uniform in $x_1$ and $x_2$ and stretched in $x_3$ so as to resolve viscous boundary layers at the bottom wall and top surface. These results imply that LES-NWM is able to perform well in capturing the strength of the full-depth upwelling and downwelling limbs of the Langmuir cells. Furthermore, the strength of these limbs and resulting deviation of mean velocity from the log law is nearly independent of horizontal domain length and cell meanderings.

Figure (5) shows root mean square (rms) of velocity. Results from LES-NWM with

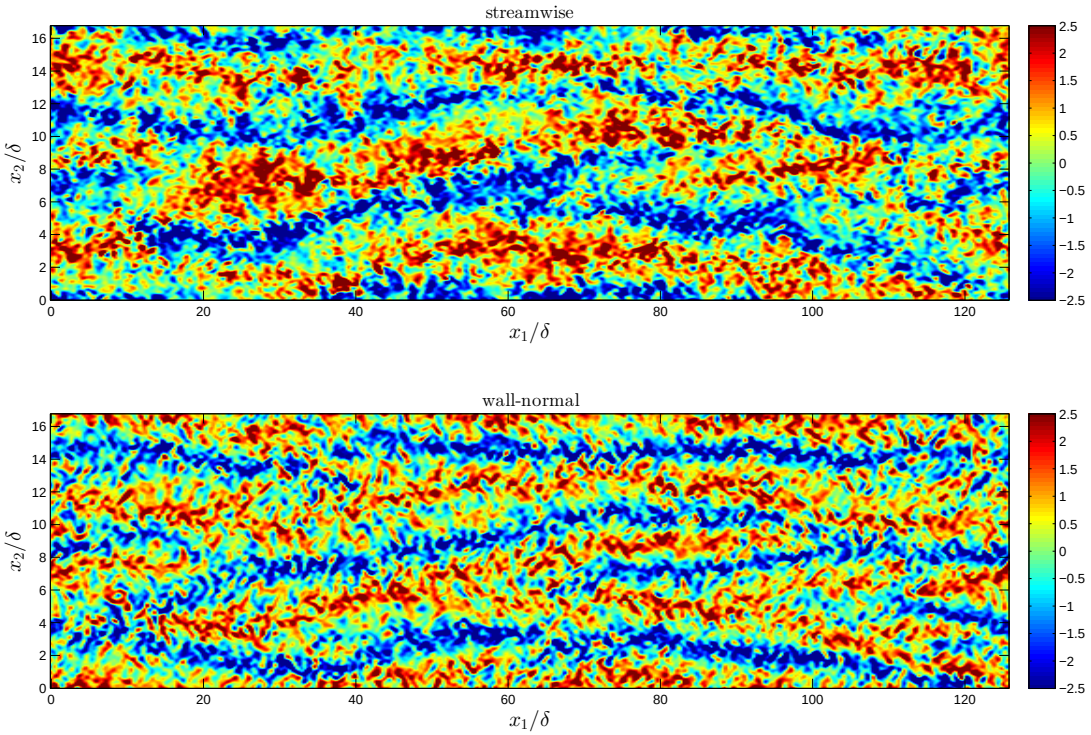


**Figure 3**: Mid-depth ($x_3 = \delta$) streamwise-spanwise plane of instantaneous streamwise (top) and wall-normal (bottom) velocity fluctuations scaled by $u_\tau$ from LES-NWM in the domain $L_1\delta \times L_2/\delta \times L_3/\delta = 40\pi \times \frac{16}{3}\pi \times 2$. Results were obtained with classical wall model in sub-section 3.1 with $B = 6.5$ in (2).

the classic wall model in sub-section 3.1 and different domain lengths in $x_1$ and $x_2$ do not show significant differences in streamwise, spanwise and wall-normal velocity rms ($u_1$-rms, $u_2$-rms, $u_3$-rms, respectively). In Figure (5; left panel) the near-bottom peak in $u_1$-rms predicted by LES-NWM with the classic wall model on the smallest domain listed in Table 1 is significantly higher than the peak predicted by LES-NWR on the same domain. This could potentially be due to the under-resolution of the LES-NWM compared with the LES-NWR in the streamwise direction. The significant non-zero $u_2$-rms Figure (5; middle panel) at the bottom wall is an artifact of the wall slip velocity associated with the classic wall model. This non-zero $u_2$-rms at the wall may simply be over-written with a zero.

As mentioned earlier, the LES-NWM results of Figures (4) and (5) were obtained with the classic wall model described in sub-section 3.1. Cases (not shown here) were run with different values of $B$ in equation (2), given the deviation from the log-law induced by the Langmuir cells. For example, a case with $B = 5.5$ did not yield significant differences from the mean velocity and rms of velocity profiles in Figures (4) and (5) obtained with $B = 6.5$.

Finally, Figure (6) shows a comparison between LES-NWM with the classic wall model

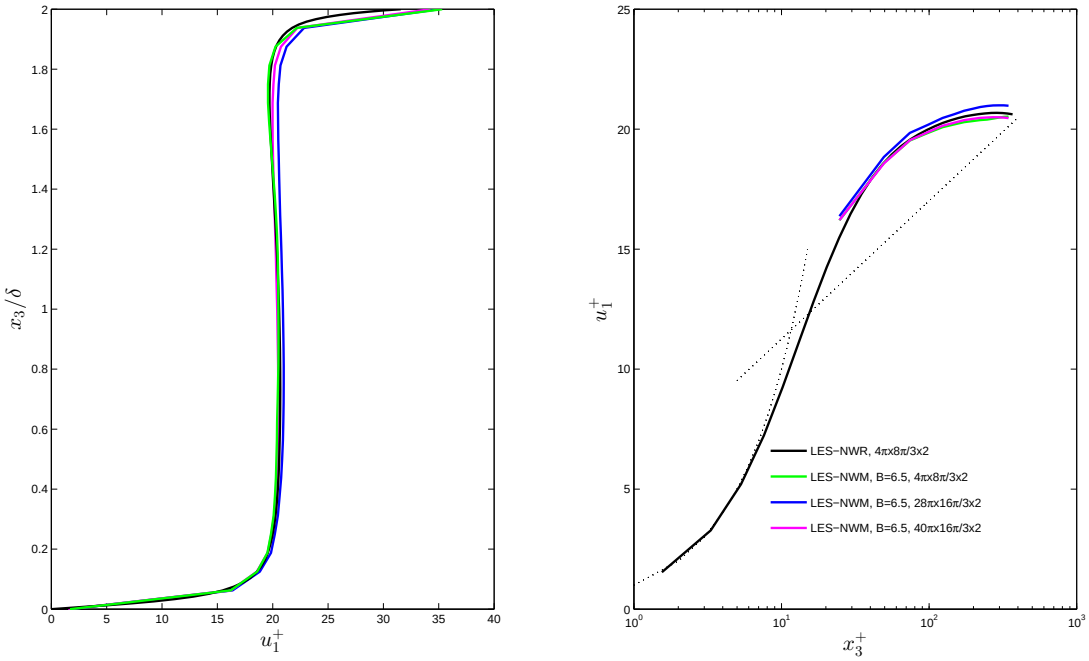


**Figure 4**: Mean velocity in regular units (left) and plus units (right) for LES-NWM in domains of various lengths. Domain lengths are specified in the figure legend in dimensionless units. Results were obtained with classical wall model in sub-section 3.1 with $B = 6.5$ in (2). Distance to the bottom wall in plus units is defined as $x_3^+ = x_3 u_\tau/\delta$.

described in sub-section 3.1 and the weak imposition of the no-slip bottom described in sub-section 3.2. The weak no-slip bottom boundary condition leads to under-prediction of the near-bottom $u_1$-rms and $u_2$-rms peaks relative to the classic wall model, perhaps due to damping of near-wall fluctuations by the penalty term (i.e. the third term on the right hand side) in equation (3). Differences between the mean velocity predicted by these two near-wall treatments were not significant (not shown) and thus both wall models are able to accurately predict the strength of upwelling and downwelling limbs of full-depth Langmuir cells.

## 5 CONCLUSIONS

This paper presented results from LES-NWM of Langmuir turbulence in shallow water characterized by full-depth Langmuir circulation. LES-NWM with domain lengths sufficiently wide and long allowed for the resolution of multiple Langmuir cells and the interaction between the cells resulting in cell meanderings and thus the so-called "y-junctions". It was seen that the strength of full-depth downwelling limbs generating deviation from the log law (characteristic of the mean velocity profile of typical boundary layers) is independent of cell meanderings and thus horizontal domain lengths. This is an important

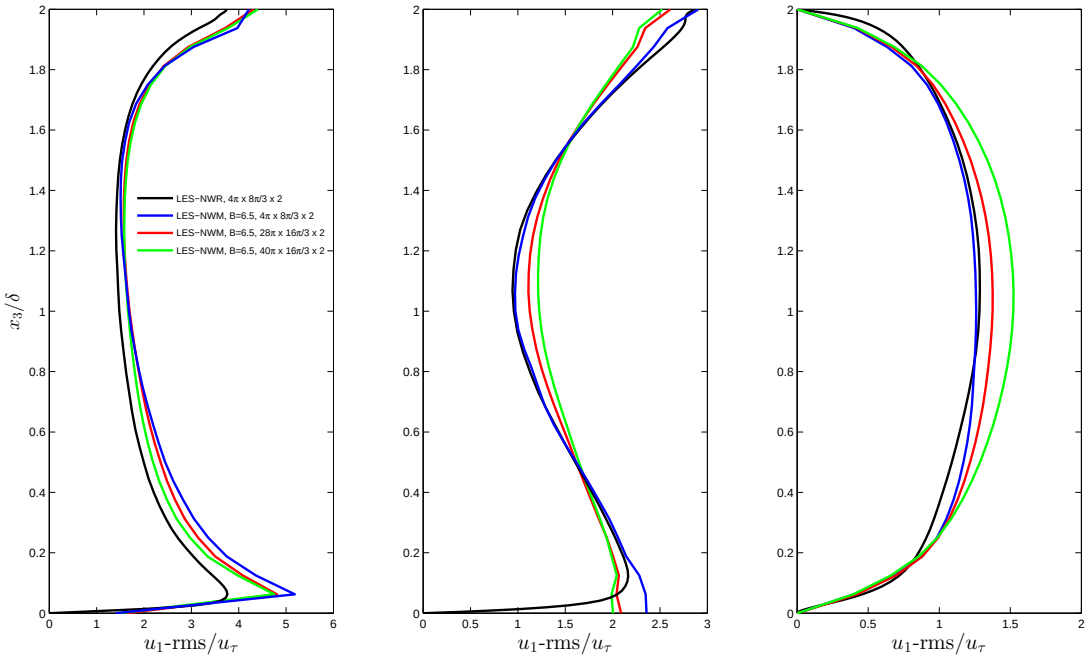


**Figure 5**: Root mean square of velocity for LES-NWM in domains of various lengths. Domain lengths are specified in the figure legend in dimensionless units. Results were obtained with classical wall model in sub-section 3.1 with $B = 6.5$ in (2).

result as it shows that future LES simulations aiming to obtain parameterizations of the strength of full-depth downwelling and upwelling limbs of Langmuir cells in terms of wind and wave forcing conditions may be performed on smaller domains capturing only one single cell and thus requiring less expensive meshes. As was shown in [13] and [8], the deviation from the log-law caused by full-depth Langmuir cells is directly proportional to the strength of the downwelling limbs. Furthermore, RANS (Reynolds-averaged Navier-Stokes) parameterizations of the vertical mixing resulting from the action of these limbs is principally dependent on their strength and thus require accurate parameterization of this strength [8]. Such a vertical mixing parameterization would be useful for inclusion in coarse-scale coastal circulation models that do not resolve the Langmuir cells yet still (up to date) use vertical mixing parameterizations that do not account for Langmuir circulation.

Langmuir cell meanderings are an important feature of lateral dispersion by Langmuir turbulence, thus LES-NWM on horizontally expanded domains should continue in order to provide a parameterization of lateral dispersion by Langmuir cells.

Finally, LES-NWM with weak imposition of the no-slip bottom condition tends to under-predict streamwise and spanwise velocity rms relative to LES-NWM with the classical wall model. However, LES-NWM with weak imposition of the no-slip bottom is

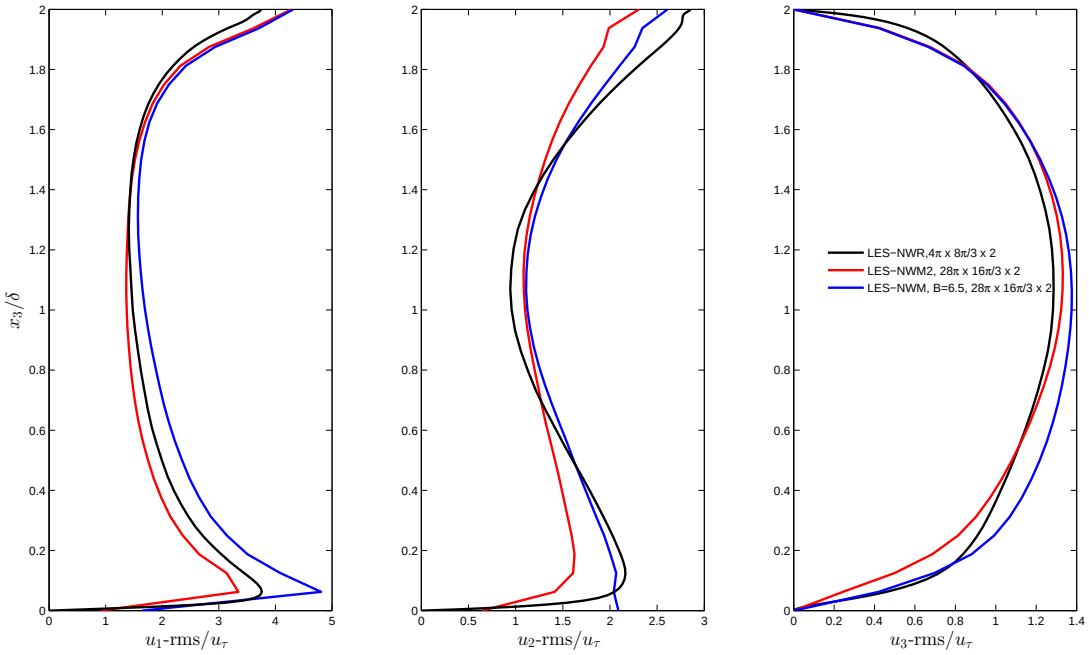


**Figure 6**: Root mean square of velocity from LES with the classical wall model in sub-section 3.1 with $B = 6.5$ in (2) (denoted as LES-NWM in the figure legend) and LES with the alternate wall treatment based on weak imposition of the no-slip bottom boundary condition in (3) (denoted as LES-NWM2 in the legend). Domain lengths are specified in the figure legend in dimensionless units.

still able to accurately represent the strength of the downwelling limbs of the Langmuir cells and thus the mean velocity log-law deviation. Current work is focusing on extending the weak imposition of the no-slip bottom to coarse-scale RANS of Langmuir turbulence that do not resolve the cells. Preliminary results have shown that weak imposition of the no-slip bottom is a viable option for these types of simulations given the observed significant dependence of classical RANS turbulence models on the $B$ coefficient in (2).

## REFERENCES

[1] Bazilevs, Y. and Calo, V. M. and Cottrel, J. A. and Hughes, T. J. R. Variational multiscale residual-based turbulence modeling for large eddy simulation of incompressible flows. *Comput. Method Appl. Eng.* (2007) **197**:173–201.

[2] Bazilevs, Y. and Michler, C. and Calo, V. M. and Hughes, T. J. R. Weak Dirichlet boundary conditions for wall-bounded turbulent flows. *Comput. Method Appl. Eng.* (2007) **196**:4853–4862.

[3] Bazilevs, Y. and Hughes, T. J. R. NURBS-based isogeometric analysis for the computation of flows about rotating components. *Comput. Mech.* (2008) **43**:143–150.

[4] Craik, A. D. D. and Leibovich, S. A rational model for Langmuir circulation. *J. Fluid. Mech.* (1976) **73**:401–426.

[5] Gargett, A. E. and Wells, J. R. and Tejada-Martínez, A. E. and Grosch, C. E. Langmuir supercells: A mechanism for sediment resuspension and transport in shallow seas. *Science* (2004) **306**:1925–1928.

[6] Gargett, A. E. and Wells, J. R. Langmuir turbulence in shallow water. Part 1. Observations *J. Fluid. Mech.* (2007) **576**:27–61.

[7] McWilliams, J. C. and Sullivan, P. P. and Moeng C-H. Langmuir turbulence in the ocean. *J. Fluid. Mech.* (1997) **334**:31–58.

[8] Sinha, N. Towards RANS parameterization of Langmuir turbulence in shallow water. Ph.D. thesis, University of South Florida (2013).

[9] Piomelli, U. and Balaras, E. Wall-layer models for large-eddy simulations. *Annu. Rev. Fluid. Mech.* (2012) **34**:349–374.

[10] Tejada-Martínez, A. E. and Akkerman, I. and Bazilevs, Y. Large-eddy simulation of shallow water Langmuir turbulence using isogeometric analysis and the residual-based variational multiscale method. *J. Appl. Mech* (2012) **34**:349–374.

[11] Thorpe, S. A. Langmuir circulation. *Annu. Rev. Fluid. Mech.* (2012) **34**:349–374.

[12] Tejada-Martínez, A. E. and Grosch, C. E. and Gargett, A. E. and Polton, J. A. and Smith, J. A. and MacKinnon, J. A. A hybrid spectral/finite-difference large-eddy simulator of turbulent processes in the upper ocean. *Ocean Model.* (2009) **39**:115–142.

[13] A. E. Tejada-Martínez and Grosch, C.E. and Sinha, .N and Akan, C. and Martinat, G. Disruption of bottom log layer in large-eddy simulations of full-depth Langmuir circulation. *J. Fluid. Mech.* (2012) **699**:79–93.